AIAA JOURNAL
Vol. 35, No. 1, January 1997

Coupling Between a Supersonic Turbulent Boundary Layer and a Flexible Structure

Abdelkader Frendi*
Analytical Services and Materials, Inc., Hampton, Virginia 23666

A mathematical model and a computer code have been developed to fully couple the vibration of an aircraft fuselage panel to the surrounding flowfield, turbulent boundary layer, and acoustic fluid. The turbulent boundary-layer model is derived using a triple decomposition of the flow variables and applying a conditional averaging to the resulting equations. Linearized panel and acoustic equations are used. Results from this model are in good agreement with existing experimental and numerical data. It is shown that in the supersonic regime full coupling of the flexible panel leads to lower response and radiation from the panel. This is believed to be due to an increase in acoustic damping on the panel in this regime. Increasing the Mach number increases the acoustic damping, which is in agreement with earlier work.

I. Introduction

FUTURE civilian aircraft, subsonic or supersonic, will have to be quieter, more fuel efficient, less expensive, and faster than today's aircraft. In light of these stringent requirements, a substantial amount of research and development work needs to be accomplished in various engineering fields. With the renewed interest in the development of a high-speed civil transport aircraft, research interests have been increasing in the area of interior noise and sonic fatigue.

The source of aircraft interior noise is generally the vibrations of the outer skin of the fuselage. These vibrations are in turn caused by the pressure fluctuations in the mostly turbulent boundary layer on the aircraft. Therefore, to reduce the interior noise level, it is imperative that we understand the mechanisms by which noise is transmitted from the turbulent boundary layer to the interior. This is a challenging problem as it involves a fluid mechanics phenomenon, turbulence, that is the least understood in fluid mechanics.

Early work on the effects of turbulent boundary-layer pressure fluctuations on structural vibration and interior noise generation focused mainly on the structure and used either experimental data or empirical models to describe the pressure field in the turbulent boundary layer. One of the widely used models in the literature is the Corcos model.[1]

This model was derived based on experimental observations and gives the cross spectral density of the pressure as

$$\Gamma(\zeta, \eta, \omega) = \Phi(\omega) A(\omega\zeta/U_c) B(\omega\eta/U_c) \exp[-j(\omega\zeta/U_c)] \quad (1)$$

where $\Phi(\omega)$ describes the frequency content (or autospectrum); A and B, the spatial distribution and the exponential term, represent the convection of the pressure field. In the preceding equation, ω is the frequency, ζ and η are the streamwise and spanwise separation distances, and U_c is the convection velocity. Based on the experiments of Willmarth and Wooldridge,[2] the functions A and B were represented by decaying exponentials of the form

$$A(\omega\zeta/U_c) = \exp(-\alpha|\omega\zeta/U_c|)$$
$$B(\omega\eta/U_c) = \exp(-\beta|\omega\eta/U_c|) \quad (2)$$

where the constants α and β are arbitrary and are chosen to fit a given set of experimental data.

Presented as Paper 96-0433 at the AIAA 33rd Aerospace Sciences Meeting, Reno, NV, Jan. 15–18, 1996; received Feb. 2, 1996; revision received Sept. 18, 1996; accepted for publication Sept. 26, 1996; also published in *AIAA Journal on Disc*, Volume 2, Number 2.

*Senior Research Scientist. Member AIAA.

In recent years, many improvements of the original Corcos' model have been proposed.[3–10] Graham[11] performed a comparative study of the various models and concluded that, for aircraft interior noise problems, Corcos' model is inadequate because of its inability to account for the dependence of the correlation length on boundary-layer thickness. He recommended that the Efimtsov extension of the Corcos model be used for such problems. The superior performance of the Efimtsov model was attributed to the fact that this model was derived from aircraft data rather than laboratory experiments. In addition to these models, several studies used the Monte Carlo method to solve this problem.[12–14] This approach idealized the boundary-layer pressure field to be a homogeneous, multidimensional Gaussian random process with zero mean.

It is important to emphasize that all of the aforementioned models need experimental data to determine the various constants and become useful. Since surface pressure data are difficult to obtain experimentally, especially for compressible high-speed flows, the use of these models is further limited. In addition, once the constants are determined, the pressure field in the turbulent boundary layer is fixed and the structure–fluid interaction problem is therefore decoupled. This approach can be useful in some engineering problems where coupling is not important (low speeds); however, at supersonic speeds the coupling between fluid and structure is very important. As was shown by Lyle and Dowell,[15] acoustic damping on the structure becomes dominant as the speed is increased from subsonic to supersonic. This is further confirmed by the calculations of Wu and Maestrello,[16] who showed that in a supersonic regime neglecting the coupling term leads to an overestimate of the structural response at higher modes.

To account for the various fluid–structure interaction effects, one needs to solve the complete set of partial differential equations for the fluid and the structure with the appropriate boundary conditions. The fluid motion is described by the nonlinear Navier–Stokes equations, and the structural response is given by the nonlinear plate equations. This coupled system of equations is extremely difficult to solve even with the powerful, modern computers. It is therefore necessary to simplify this system of equations. In recent years, scientists in fluid dynamics have developed a simplified form of the Navier–Stokes equations. This new approach is known as the large-eddy simulation (or simply LES). The grids used in LES calculations are coarser than those used in direct numerical simulation (DNS; full Navier–Stokes); therefore the scales resolved by LES have a lower limit, which is the grid size. The contribution of the scales smaller than the grid size is modeled. One of the first LES models was introduced by Smagorinsky[17] in the early 1960s. This model performs reasonably well in free shear layers but does a poor job in wall bounded flows, i.e., boundary layers. Recently new models have been developed using the Smagorinsky idea but with more physical insight.[18–20] However, these new models have yet to be applied to

realistic engineering problems. In addition, from a computational viewpoint, an LES calculation is only an order of magnitude faster than an equivalent DNS calculation. Therefore, this approach is still not viable for the solution of engineering problems.

Over a century ago, Reynolds[21] proposed a decomposition of the turbulent flow quantities into a time-averaged mean, denoted by an overbar, and a fluctuation:

$$f = \bar{f} + f' \tag{3}$$

Using this decomposition, he derived a new set of equations for the mean quantities where the contribution from the turbulent fluctuations had to be modeled. These new equations became known as the Reynolds-averaged Navier–Stokes (RANS) equations and have been used to solve a wide variety of engineering problems. Since these equations are derived only for the mean quantities, they cannot provide any information on the dynamics of the flow. To overcome this deficiency, Hussain and Reynolds[22,23] and Reynolds and Hussain[24] used a triple decomposition of the form

$$f = \bar{f} + \hat{f} + f'' \tag{4}$$

to study small-amplitude wave disturbances in turbulent shear flows. In Eq. (4), $\hat{f}$ represents the wave motion and f'' is the turbulent fluctuation. A combination of time and conditional averaging were used to arrive at a set of dynamic equations describing the wave motion. Liu[25] used a similar approach to study the near-field jet noise due to the large-scale wavelike eddies. Merkine and Liu[26] studied the development of noise-producing large-scale wavelike eddies in a plane turbulent jet. Liu and Merkine,[27] Alper and Liu,[28] and Gatski and Liu[29] studied the interactions between large-scale structures and fine-grained turbulence in a free shear flow. Gatski[30] calculated the sound production due to large-scale coherent structures in a free turbulent shear layer. More recently, Bastin et al.[31] used a semideterministic modeling approach coupled with Lighthill's acoustic analogy to calculate the jet mixing noise from unsteady coherent structures.

In the last few years, numerous advanced turbulence models have been developed that led to the solution of a wide variety of engineering problems. The extension of the RANS method to unsteady problems has been made less difficult with the new models because they contain more physics. The unsteady RANS method has been identified by many researchers as being equivalent to a very large eddy simulation (VLES).[32] The advantages of using VLES are as follows: it is computationally less costly than either LES or DNS, the models have been tested extensively, and the method can be used for any geometry, etc.

The remainder of this paper is organized as follows. In Sec. II the mathematical model is described, Sec. III describes the method of solution used to solve the model, the results and discussions are given in Sec. IV, and a summary of the results and some concluding remarks are given in Sec. V.

II. Mathematical Model

A. Turbulent Boundary-Layer Equations

Using the triple decomposition proposed by Reynolds and Hussain,[24] the flow quantities are decomposed as follows:

$$g = \tilde{g} + \hat{g} + g'' \tag{4}$$

where g represents a flow quantity and $(\tilde{g})$ its Favre-averaged mean defined by

$$\tilde{g} = \overline{(\rho g)}/\bar{\rho} \tag{5}$$

When decomposing the density, the turbulent fluctuations ρ'' are neglected by virtue of Morkovin's hypothesis,[33] which has been recently verified by Sommer et al.[34]; therefore

$$\rho = \bar{\rho} + \hat{\rho} \tag{6}$$

In Eqs. (4) and (6), $(\hat{g}, \hat{\rho})$ is the low-frequency variation part of the mean and (g'') is the turbulent fluctuation.

By defining the total mean to be

$$G = \tilde{g} + \hat{g} \tag{7}$$

Eq. (4) becomes

$$g = G + g'' \tag{8}$$

Equation (8) has a form similar to that of Eq. (3); the only difference is that in Eq. (3) $\bar{f}$ is a time independent mean whereas in Eq. (8) G is time dependent.

In the derivation of the dynamic equations used by Reynolds, a conditional averaging was introduced. Some properties of this averaging are

$$\begin{gathered} \langle g'' \rangle = 0 \qquad \langle \hat{g} f \rangle = \hat{g} \langle f \rangle \qquad \langle \tilde{g} f \rangle = \tilde{g} \langle f \rangle \\ \langle \tilde{g} \rangle = \tilde{g} = \langle \tilde{g} \rangle \qquad \widetilde{g f''} = \langle \widetilde{g f''} \rangle = 0 \end{gathered} \tag{9}$$

Using the decomposition given by Eq. (8) in the continuity, momentum, energy, and state equations along with the conditional averaging and Einstein summation convention, one arrives at the following mass, momentum, energy, and state equations:

$$\frac{\partial \rho}{\partial t} + \frac{\partial}{\partial x_i}(\rho U_i) = 0, \qquad i = 1, 2, 3 \tag{10}$$

$$\frac{\partial}{\partial t}(\rho U_i) + \frac{\partial}{\partial x_j}[\rho U_i U_j - \langle \tau_{ij} \rangle + \rho \langle u_i'' u_j'' \rangle] + \frac{\partial P}{\partial x_i} = 0 \qquad i, j = 1, 2, 3 \tag{11}$$

$$\begin{aligned} \frac{\partial E}{\partial t} + \frac{\partial}{\partial x_j}[(E + P)U_j - \langle \tau_{ij} \rangle U_j + \langle e'' u_j'' \rangle \\ + \langle p'' u_j'' \rangle - \langle \tau_{ij} u_j'' \rangle] = 0 \end{aligned} \tag{12}$$

$$\begin{aligned} P = (\gamma - 1)\{E - \rho[U_1^2 + U_2^2 + U_3^2 + \langle u_1'' \rangle^2 \\ + \langle u_2'' \rangle^2 + \langle u_3'' \rangle^2]/2\} \end{aligned} \tag{13}$$

In Eqs. (10–13), (ρ, U_i, E, P) represent the total means of the variables (ρ, u_i, e, p), whereas (u_i'', u_j'', e'', p'') are the turbulent fluctuations. The variable e is the total energy defined as $e = p/(\gamma - 1) + \rho(u_1^2 + u_2^2 + u_3^2)/2$. In Eqs. (11) and (12), $\langle \tau_{ij} \rangle$ is the conditionally averaged stress tensor,

$$\langle \tau_{ij} \rangle = \frac{M_\infty}{Re_L}\left[\mu\left(\frac{\partial U_i}{\partial x_j} + \frac{\partial U_j}{\partial x_i}\right) - \frac{2}{3}\mu \frac{\partial U_k}{\partial x_k}\delta_{ij}\right] \tag{14}$$

where M_∞, Re_L, and μ are the freestream Mach number, Reynolds number, and molecular viscosity, respectively. The term $\langle u_i'' u_j'' \rangle$ of Eq. (11) is similar to the Reynolds stress tensor and is modeled in the same way. In Eq. (12), $\langle e'' u_j'' \rangle$, $\langle p'' u_j'' \rangle$, and $\langle \tau_{ij} u_j'' \rangle$ have to be modeled.

Invoking the Boussinesq approximation that the Reynolds stress tensor is proportional to the mean strain-rate tensor leads to

$$\rho \langle u_i'' u_j'' \rangle = \tfrac{2}{3}\rho k \delta_{ij} - 2\mu_t (S_{ij} - \tfrac{1}{3} S_{kk} \delta_{ij}) \tag{15}$$

where $k = \langle u_i'' u_i'' \rangle / 2$ is the turbulent kinetic energy, μ_t is the turbulent eddy viscosity, and S_{ij} is the mean strain-rate tensor given by

$$S_{ij} = \frac{1}{2}\left[\frac{\partial U_i}{\partial x_j} + \frac{\partial U_j}{\partial x_i}\right] \tag{16}$$

The turbulent eddy viscosity is obtained from the relation

$$\mu_t = C_\mu^* (\rho k / \omega) \tag{17}$$

where C_μ^* is a constant and ω is the specific dissipation rate (ϵ / k) with ϵ being the dissipation.

The conservation equations for k and ω are

$$\frac{\partial}{\partial t}(\rho k) + \frac{\partial}{\partial x_j}(\rho U_j k) = -\rho\langle u_i' u_j'\rangle \frac{\partial U_i}{\partial x_j} - \rho\omega k + \frac{\partial}{\partial x_j}\left(\frac{\mu_{tl}}{\sigma_k}\frac{\partial k}{\partial x_j}\right) \tag{18}$$

$$\frac{\partial}{\partial t}(\rho\omega) + \frac{\partial}{\partial x_j}(\rho U_j \omega) = -\rho C_{\omega_1}\frac{\omega}{k}\langle u_i' u_j'\rangle \frac{\partial U_i}{\partial x_j} - C_{\omega_2}\rho\omega^2 + \frac{\partial}{\partial x_j}\left(\frac{\mu_{tl}}{\sigma_\omega}\frac{\partial \omega}{\partial x_j}\right) \tag{19}$$

In Eqs. (18) and (19), $\mu_{tl} = C_{\mu l}^{*}\rho(k/\omega)$ and $C_{\omega_1} = C_{\omega_2} - \kappa^2/[(C_{\mu l}^{*})^{0.5}\sigma_\omega]$, with $C_{\mu l}^{*} = 0.09$ (same as C_μ^{*} in the log layer), $\sigma_k = \sigma_\omega = 2$, $C_{\omega_2} = 0.83$, and $\kappa = 0.41$. The model described earlier was derived by Wilcox[35] and is known as the (k-ω) turbulence model.

B. Plate Equation

The out-of-plane plate displacement w is given by the biharmonic equation

$$D\Delta^2 w + \rho_p h\frac{\partial^2 w}{\partial t^2} + \Gamma\frac{\partial w}{\partial t} = \delta p \tag{20}$$

where D is the plate stiffness obtained from $D = E_p h^3/12(1-\nu_p^2)$, with E_p being the Young modulus, h the plate thickness, and ν_p the Poisson ratio. In Eq. (20), ρ_p is the plate material density and Γ is the structural damping. The biharmonic term is defined as

$$\Delta^2 = \frac{\partial^4}{\partial x^4} + 2\frac{\partial^4}{\partial x^2\partial y^2} + \frac{\partial^4}{\partial y^4} \tag{21}$$

The right-hand side, δp, of Eq. (20) represents the pressure loading due to the adjacent fluids and can be written as

$$\delta p = p^a - p^{bl} \tag{22}$$

with p^a being the radiated acoustic pressure and p^{bl} the turbulent boundary-layer pressure calculated from the model in Sec. II.A.

C. Acoustic Radiation Equation

To calculate the pressure p^a of Eq. (22), Kirchhoff's formula is used to arrive at (see Ref. 36 for details)

$$p^a(x, y, z, t) = \frac{\rho_\infty}{2\pi}\int\int_D \frac{[w_{tt}(\tau, x', z')]}{R}\,dx'dz' \tag{23}$$

where the integration domain D is the whole plate and $w_{tt} = \partial^2 w/\partial t^2$. In Eq. (23), the square brackets, [ ], are used to denote a retarded time, i.e.,

$$[w_{tt}(\tau, x', z')] = w_{tt}(t - R/c_\infty, x', z') \tag{24}$$

where $R = [(x-x')^2 + y^2 + (z-z')^2]^{1/2}$ is the distance from an observer point (x, y, z) to a point on the plate $(x', 0, z')$. In Eq. (24), c_∞ is the speed of sound. Equation (23) is used to calculate the pressure both on the surface of the plate and in the far field. When using Eq. (23) to calculate the surface pressure, a Taylor series expansion of the integrand is used to avoid the singularity at $R = 0$ (when the observer point coincides with the source).

III. Method of Solution

The turbulent boundary-layer equations are solved using the three-dimensional thin-layer Navier–Stokes code known as CFL3D.[37] The numerical method uses a second-order accurate finite volume scheme. The convective terms are discretized with an upwind scheme that is based on Roe's flux difference splitting method, whereas all of the viscous terms are centrally differenced. The equations are integrated in time with an implicit, spatially split approximate-factorization scheme. The thin-layer approximation retains only those viscous terms with derivatives normal to the body surface. This is generally considered to be a good approximation for high-Reynolds-number aerodynamic flows with minimal separation. Two calculations are made for each case; first the steady-state mean velocity profiles are obtained using a large domain that includes the leading edge of the plate, and then using a smaller domain downstream of the leading edge an unsteady calculation is carried out by perturbing the mean velocity profile at the inflow boundary as follows:

$$u = \tilde{u} + \epsilon R_n(y, z, t) \tag{25}$$

In Eq. (25), $R_n(y, z, t)$ is a random number generated using an International Mathematical and Statistical Libraries routine called RNNOF[38] and ϵ is a small amplitude chosen to be between 0.05 and 0.25. In the steady-state calculation, the flow in the region upstream of the plate's leading edge is specified as laminar, whereas that downstream of the leading edge is turbulent. The plate equation (20) is integrated using an implicit finite difference method for structural dynamics developed by Hoff and Pahl.[39] The radiated acoustic pressure p^a is obtained through a combination of the Simpson and trapezoidal rules of integration in the (x, z) directions.[36]

Coupling between the plate and the acoustic and boundary-layer pressure fields is obtained as follows. Using the previous time step plate velocity and acceleration as boundary conditions, the turbulent boundary-layer equations (10–13), (18), and (19) and the acoustic equation (23) are integrated to obtain the new surface pressure fields; these are then used to update the plate equation. This procedure is repeated at every time step. Figure 1 shows a two-dimensional computational domain with the different mathematical models. The top domain shows the presence of a leading-edge shock, because all of the cases studied are supersonic. In the following results, the flexible plate is clamped between two rigid ones except in one case where the plate is simply supported.

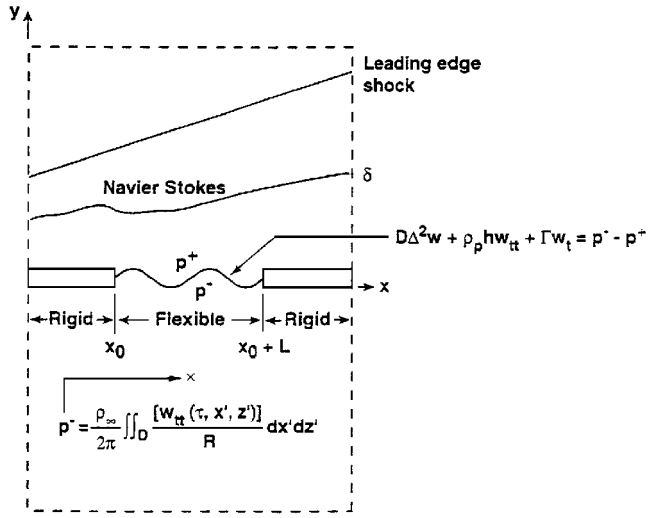

Fig. 1 Two-dimensional computational domain and the mathematical model.

IV. Results and Discussions

This section is divided into several subsections. In Sec. IV.A, results from a typical fully coupled run are presented. Comparisons to existing experimental data are given in Sec. IV.B. In Sec. IV.C, results from two runs at two different Mach numbers are given, and finally in Sec. IV.D, the effects of plate boundary conditions on the response and acoustic radiation are analyzed.

A. Results from a Typical Fully Coupled Case

The flow and structural properties used in this case are taken from Maestrello.[40] The mean flow parameters are $M_\infty = 1.98$ (freestream Mach number), $T_t = 563$ R (total temperature), $T_w = 550$ R (wall temperature), and $Re/\text{ft} = 3.73 \times 10^6$ (Reynolds number per foot). A titanium plate is used in this study with the following parameters: length $a = 12$ in., width $b = 6$ in., thickness $h = 0.062$ in., density per unit area $\rho_p h = 2.315 \times 10^{-5}$ lbf s^2/in.^{3},

stiffness $D = 345$ lbf $\cdot$ in., and damping $\Gamma = 7.4 \times 10^{-4}$ lbf $\cdot$ s/in.^{3}. The parameter ϵ of Eq. (25) is set to 0.25. The plate is oriented such that the length a is along the streamwise direction.

The computational domain used is $2 \times 1 \times 2$ ft in the streamwise, spanwise, and vertical directions, respectively. The number of points used in the respective directions are $83 \times 53 \times 83$. Equally spaced points are used in the streamwise and spanwise directions, whereas grid stretching is used in the vertical direction. The leading edge of the plate is 0.5 ft upstream of the inflow boundary. For each case studied, the second grid point in the vertical direction is located at a $y^+ < 1$, where y^+ is a nondimensional coordinate given by $y^+ = yu_\tau/\nu$ with $u_\tau = (\tau_w/\rho)^{0.5}$ being the friction velocity, ν the kinematic viscosity, and ρ the density. In the u_τ expression, τ_w is the wall shear stress.

Figures 2a–2c show the power spectral densities (PSDs) of the turbulent boundary-layer surface pressure at the center of the flexible plate, the center plate displacement, and the radiated pressure 1 ft away from the plate center, respectively. The PSD of the turbulent boundary-layer surface pressure shows the presence of a broad peak at around 5000 Hz (see Fig. 2a). The level decreases slowly with decreasing frequency from the peak, whereas above 5000 Hz the level decreases sharply with increasing frequency. Grid refinement and time step refinement show little effect on the location of the peak. The PSD of the displacement response at the center of the plate (Fig. 2b) shows the presence of several peaks corresponding to the various response modes of the plate. This response is dominated by the first mode, which is the (1, 1) mode located near 430 Hz. Figure 2c shows the PSD of the radiated pressure 1 ft away from the center of the plate. The frequency content of this radiated field is dominated by two plate mode frequencies, one corresponding to the (1, 1) mode and the other to the (5, 1) mode. Other intermediate frequencies are also present but at a much lower level. This result is of great significance from a noise control point of view. This means that controlling the vibration of the plate at a few natural frequencies can reduce the noise level significantly. The probability distributions of the input pressure (Fig. 3a) the displacement response (Fig. 3b) and the radiated pressure (Fig. 3c) show a Gaussian-like behavior. The cross-correlation function of the surface pressure is defined as

$$R_{pp}(\zeta, \eta, \tau) = \frac{\overline{p(x, z, t)\, p(x + \zeta, z + \eta, t + \tau)}}{\bar{p}^2} \qquad (26)$$

where ζ and η are the streamwise and spanwise separation distances and τ the time separation. The streamwise two-point correlation is obtained from Eq. (26) by setting (η, τ) to zero. Similarly, the spanwise two-point correlation and the autocorrelation are obtained by setting (ζ, τ) and (ζ, η) to zero, respectively. Figures 4a and 4b show the streamwise and spanwise two-point correlations. Both figures show that as the separation distance increases, the correlation function decreases rapidly to nearly zero, indicating the lack of correlation between the pressures at various points. Figure 5 shows the auto-correlation as a function of time. The autocorrelation decreases to zero very rapidly as time increases. Both the two-point correlations and autocorrelation behave in a manner that is characteristic of a turbulent boundary layer. Figure 6 shows a complicated instantaneous displacement response of the plate.

B. Comparisons to Experiments

Maestrello's data[40] are used for the various comparisons. The mean flow parameters used are Mach number $M_\infty = 3.03$, total temperature $T_t = 567$ R, and a Reynolds number per foot $Re/\text{ft} = 4.265 \times 10^6$. The plate parameters are the same as those given in Sec. IV.A, and the parameter ϵ is set to 0.25. Figure 7 shows the mean velocity profile ($u^+ = u/u_\tau$ vs $y^+ = yu_\tau/\nu$). There is no experimental data point for y^+ less than 60; this is due to the difficulty in making near-wall measurements. The agreement between Maestrello's data and the numerical results in the logarithmic layer region is good. In addition, the profile shows a linear behavior in the sublayer region near the wall that is a characteristic of a turbulent boundary-layer velocity profile. Figure 8 shows the PSD of the center plate displacement response obtained experimentally and numerically. The experimental results show that the response is

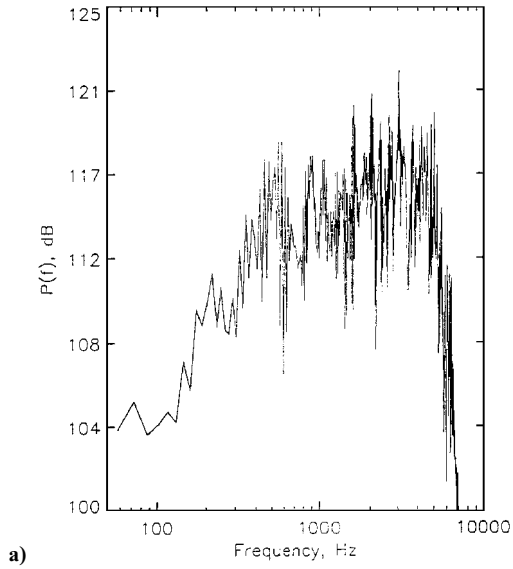

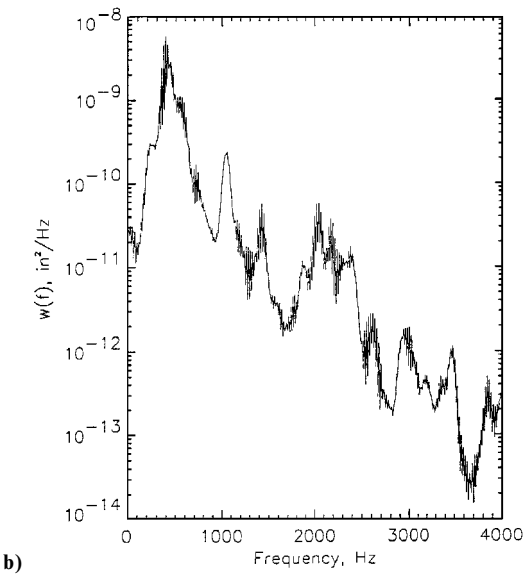

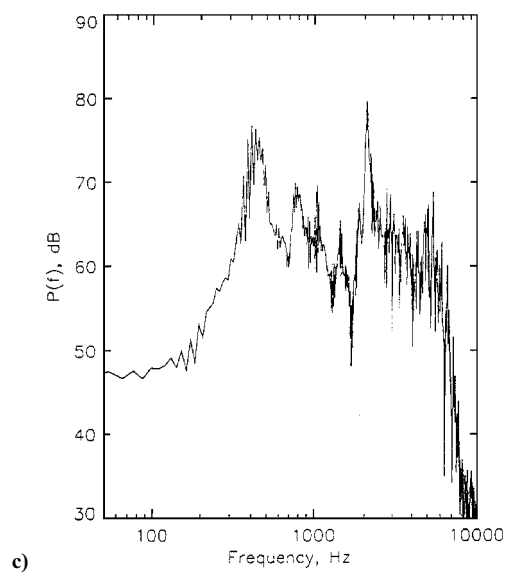

Fig. 2 PSD of a) the turbulent boundary-layer surface pressure at the center of the plate, b) the center plate displacement response, and c) the radiated pressure 1 ft away from the plate center.

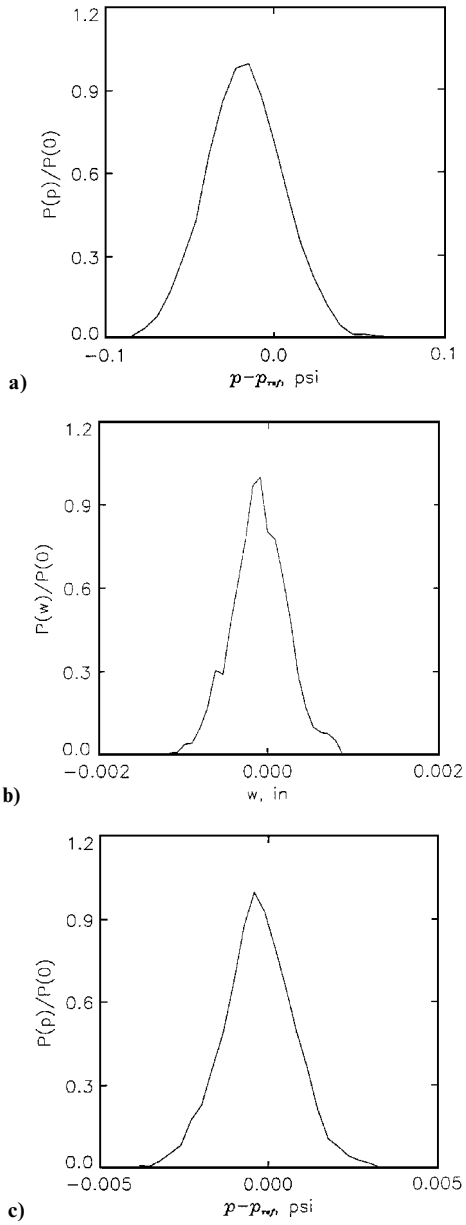

Fig. 3 Probability distribution of a) the turbulent boundary-layer surface pressure at the center of the plate, b) the center plate displacement response, and c) the radiated pressure 1 ft away from the plate center.

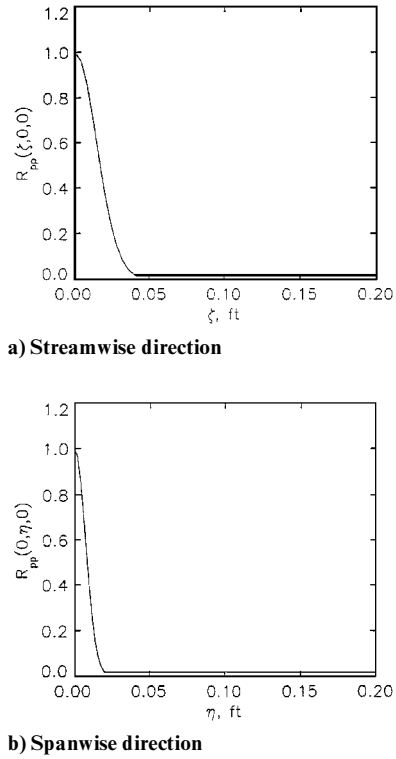

Fig. 4 Two-point correlations of the wall pressure.

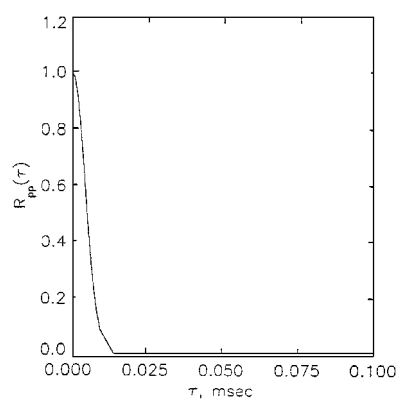

Fig. 5 Autocorrelation of the wall pressure.

dominated by the (1, 1) and (3, 1) modes. The numerical results also show the dominance of the same two modes. The agreement between the numerical and experimental results is good at the lower modes; however, the numerical results overpredict the response at higher modes. This is due to the numerical technique used to integrate the plate equation and the number of grid points used on the plate. The higher modes are less resolved and therefore show a higher response.

Figure 9 shows the PSDs of the surface pressure measured at the center of the flexible plate and that calculated numerically. The PSD of the pressure measured experimentally shows an increase in level as the frequency increases until a broad peak is reached in the vicinity of 5000 Hz. At high frequencies (> 10,000 Hz) the level decreases slowly. The numerical results show a similar behavior at low frequencies; however, at high frequencies (> 6000 Hz) the level decreases rapidly. This rapid decrease in level is believed to be due to both numerical resolution and turbulence model used. Higher grid resolution and an advanced turbulence model would result in better agreement at high frequencies. Recent experimental measurements on the Concorde[41] show similar behavior of the surface pressure fluctuation to that of Maestrello.[40] The frequency of the peak level depended on the measurement's location on the fuselage. It is important to mention at this point that, based on the results presented in Sec. IV.A, the frequencies that are critical for the structure are in the range up to 2000 Hz. The numerical results of Fig. 8 show a good agreement with experiments for this frequency range. The parameter ϵ of Eq. (25) can be adjusted to obtain better agreement with experimentally determined levels.

C. Effect of Mach Number

Two Mach number cases have been studied, 1.98 and 3.03, using the mean flow properties given in the preceding sections. Figure 10 shows the PSD of the surface pressure at the center of the plate for the two cases. The two PSDs are nearly identical. The PSDs of the displacement response at the plate center show little or no difference between the two cases at low frequencies. However, at high frequencies, the response for $M_\infty = 1.98$ is higher (see Fig. 11). This is attributed to an increase in acoustic damping with increasing Mach number. Frendi and Maestrello[42] carried out an inviscid calculation using Euler equations for the fluid coupled to the plate equation. Figure 12 shows the PSD of the nondimensional plate

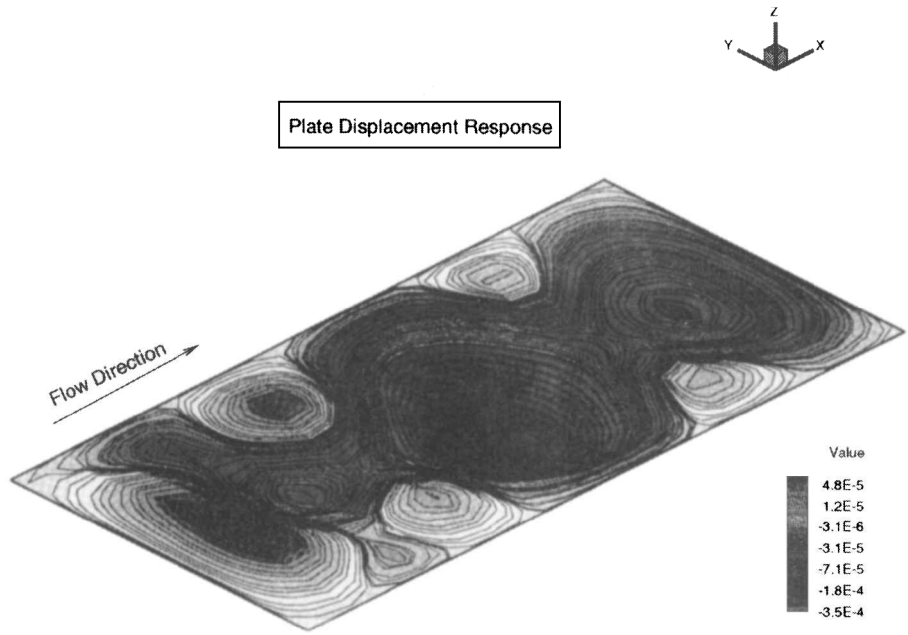

Fig. 6 Instantaneous plate displacement response.

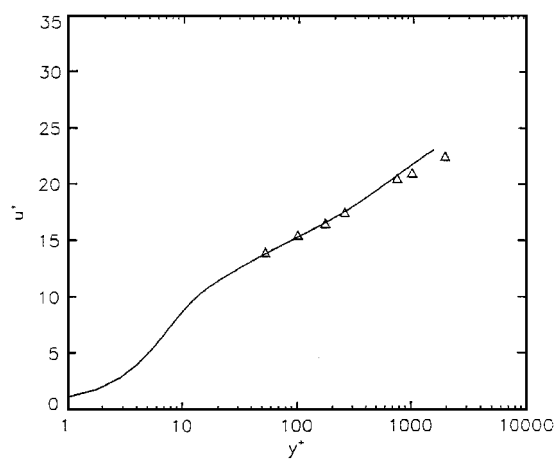

Fig. 7 Mean velocity profile: Δ, experimental results [40] and ——, numerical results.

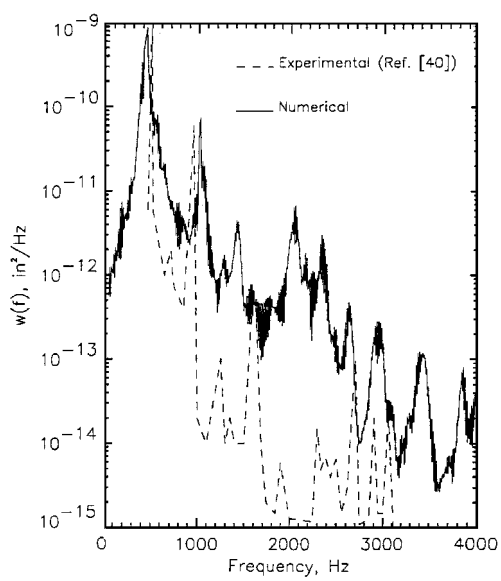

Fig. 8 Comparison of the PSD of the center plate displacement response.

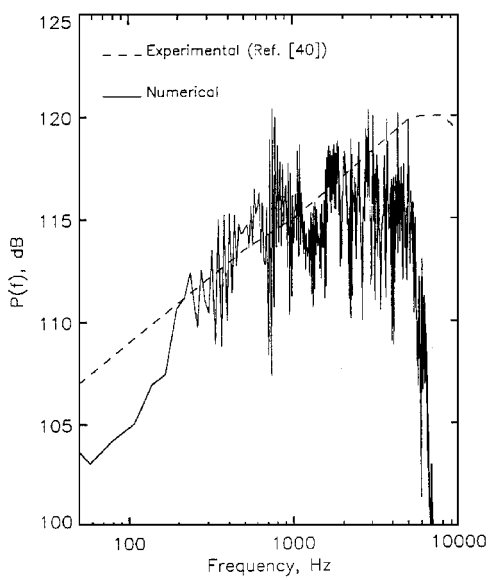

Fig. 9 Comparison of the PSD of the turbulent boundary-layer surface pressure at the center of the flexible plate.

displacement response [$\eta(f)$] they obtained at a subsonic and supersonic mean flow Mach number. The figure shows that the plate modes shift to the low frequencies (M1–M7). This shift is more pronounced at the higher modes (M3–M7) than it is at the first mode M1. They believed that this was due to an increase in acoustic damping on the plate. This result is also consistent with the results of Lyle and Dowell,[43] who showed that increasing the Mach number increases the acoustic damping on the structure. Figure 13 shows the PSDs of the radiated pressure for the two cases. Since there is little or no difference in the response at low frequencies, the radiated pressure PSDs are nearly identical.

C. Effect of Plate Edge Conditions

To access the effect of edge conditions on plate vibration and acoustic radiation, two calculations are made using the same mean flow properties as in Sec. IV.A. Figure 14 shows that the PSDs of the pressure at the center of the plate from the turbulent boundary-layer side are nearly identical. However, the PSD of the plate displacement response shows a different frequency content as expected (Fig. 15).

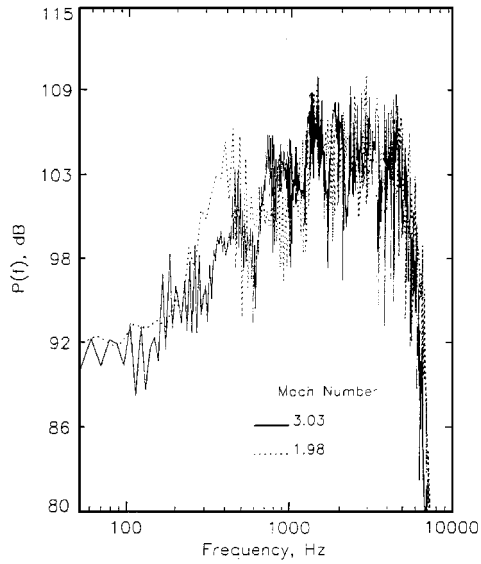

Fig. 10 Comparison of the PSDs of the surface pressure at the center of the plate for two different Mach numbers.

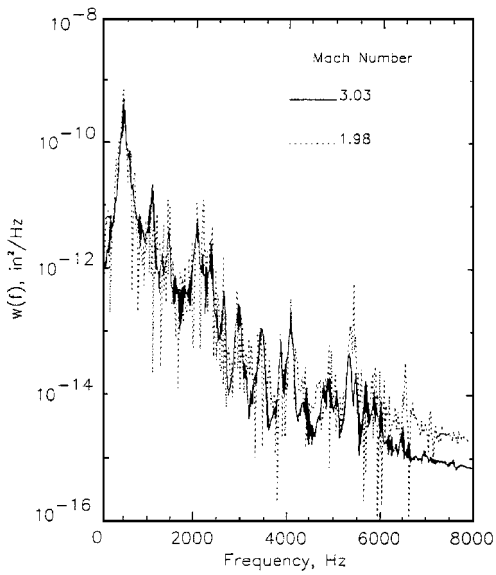

Fig. 11 Comparison of the PSDs of the center plate displacement for two different Mach numbers.

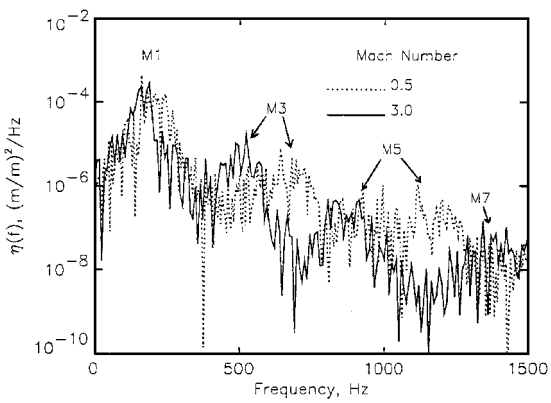

Fig. 12 PSD of the displacement response at the center of the flexible plate for mean flow Mach numbers of 0.5 and 3.0 (Ref. 42).

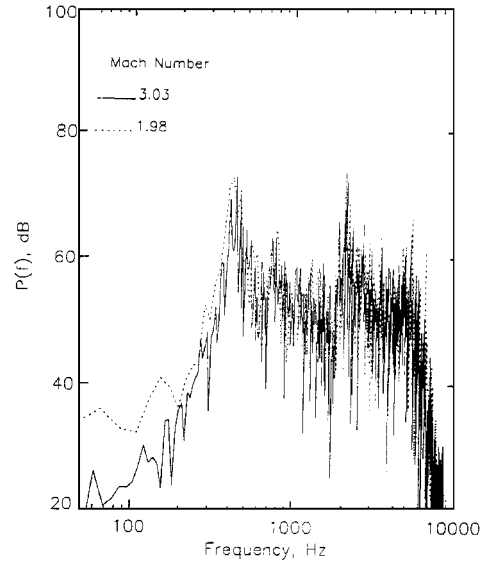

Fig. 13 Comparison of the PSDs of the radiated pressure 1 ft away from the plate for two different Mach numbers.

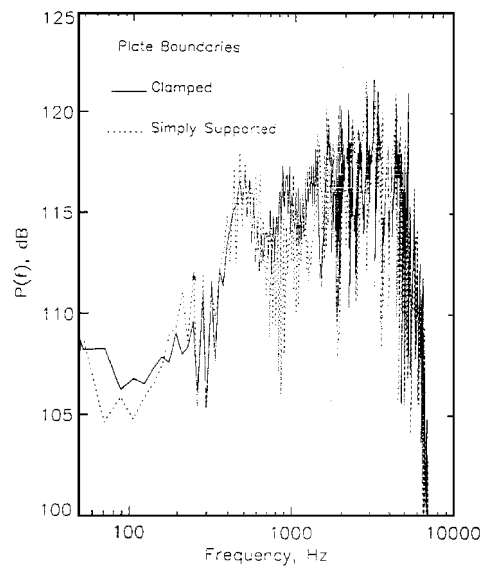

Fig. 14 Comparison of the PSDs of the surface pressure at the center of the plate for two edge conditions of the plate.

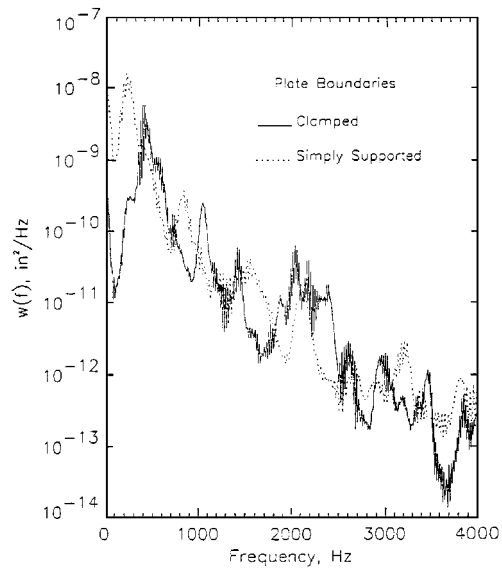

Fig. 15 Comparison of the PSDs of the center plate displacement for two edge conditions of the plate.

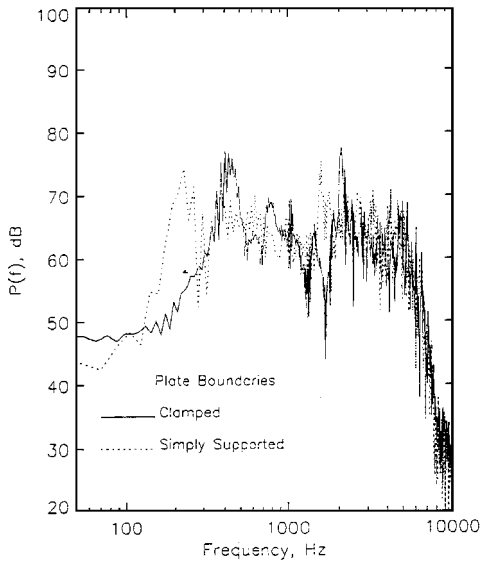

Fig. 16 Comparison of the PSDs of the radiated pressure 1 ft away from the plate for two edge conditions of the plate.

The simply supported plate shows lower natural frequencies and a higher response at the lowest modal frequency. The PSDs of the radiated pressure also show a shift in the frequency content to lower frequencies for the simply supported case. A slightly lower level is also indicated and is due mainly to lack of frequency resolution (Fig. 16). The objective of this calculation is to show the direct effect of changing any plate parameter on the radiated pressure field. Additional calculations involving changing other plate properties (such as mass, stiffness, damping, etc.) can be made using this approach to analyze their effect on the radiation field.

V. Concluding Remarks

A model that couples a supersonic turbulent boundary layer with a flexible plate and the radiated acoustic field has been developed. A three-dimensional code has been written to solve this model. The code is a modified version of CFL3D. Extensive two-dimensional and three-dimensional test calculations have been carried out. The results given by this model show good agreement with existing experimental results both for the structural response and pressure fluctuations in the turbulent boundary layer. Additional results showed the following.

1) As the Mach number increases, the acoustic damping on the plate increases. The acoustic damping lowers the response, especially for high modes.

2) Changing the boundary conditions of the plate changes the response and the radiated pressure frequency content. This shows that a computational tool can be used to assess the best noise reduction mechanisms. Further test runs can be made to support this idea.

Acknowledgments

The author would like to acknowledge the support of the Structural Acoustics Branch of NASA Langley Research Center under Contract NAS1-19700. I would like to thank Thomas Gatski for his availability to discuss the problem and the helpful advice he gave me during the course of this work.

References

[1]Corcos, G. M., "Resolution of Pressure in Turbulence," *Journal of the Acoustical Society of America*, Vol. 35, No. 2, 1963, pp. 192–198.

[2]Willmarth, W. W., and Wooldridge, C. E., "Measurements of the Fluctuating Pressure at the Wall Beneath a Thick Turbulent Boundary Layer," *Journal of Fluid Mechanics*, Vol. 14, Dec. 1962, p. 187.

[3]Ffowcs Williams, J. E., "Boundary Layer Pressures and the Corcos Model: A Development to Incorporate Low Wavenumber Constraints," *Journal of Fluid Mechanics*, Vol. 125, Dec. 1982, pp. 9–25.

[4]Chase, D. M., "Modeling the Wavenumber-Frequency Spectrum of Turbulent Boundary Layer Wall Pressure," *Journal of Sound and Vibration*, Vol. 70, No. 1, 1980, pp. 29–67.

[5]Chase, D. M., "The Character of the Turbulent Wall Pressure Spectrum at the Subconvective Wavenumbers and a Suggested Comprehensive Model," *Journal of Sound and Vibration*, Vol. 112, No. 1, 1987, pp. 125–147.

[6]Laganelli, A. L., Martellucci, A., and Shaw, L. L., "Wall Pressure Fluctuations in Attached Boundary Layer Flows," *AIAA Journal*, Vol. 21, No. 4, 1983, pp. 495–502.

[7]Laganelli, A. L., and Wolfe, H., "Prediction of Fluctuating Pressure in Attached and Separated Turbulent Boundary Layer Flow," AIAA Paper 89-1064, Oct. 1989.

[8]Blake, W. K., "Turbulent Boundary Layer Wall Pressure Fluctuations on Smooth and Rough Walls," *Journal of Fluid Mechanics*, Vol. 44, Pt. 4, 1970, pp. 637–660.

[9]Smol'yakov, A. V., and Tkachenko, V. M., "Model of a Field of Pseudosonic Turbulent Wall Pressures and Experimental Data," *Soviet Physical Acoustics*, Vol. 37, No. 6, 1991, pp. 627–631.

[10]Efimtsov, B. M., "Characteristics of the Field of Turbulent Wall Pressure Fluctuations at Large Reynolds Numbers," *Soviet Physical Acoustics*, Vol. 28, No. 4, 1982, pp. 289–292.

[11]Graham, W. R., "A Comparison of Models for the Wavenumber Frequency Spectrum of Turbulent Boundary Layer Pressures," *Proceedings of the First AIAA/CEAS Conference on Aeroacoustics* (Munich, Germany), AIAA, Washington, DC, 1994, pp. 711–720.

[12]Dowell, E. H., "Generalized Aerodynamic Forces on a Flexible Plate Undergoing Transient Motion," *Quarterly of Applied Mathematics*, Vol. 24, 1967, pp. 331–338.

[13]Shinozuka, M., "Simulation of Multivariate and Multidimensional Random Processes," *Journal of the Acoustical Society of America*, Vol. 47, No. 1, Pt. 2, 1971, pp. 357–367.

[14]Vaicaitis, R., Jan, C. M., and Shinozuka, M., "Nonlinear Panel Response from a Turbulent Boundary Layer," *AIAA Journal*, Vol. 10, No. 7, 1972, pp. 895–899.

[15]Lyle, K. H., and Dowell, E. H., "Acoustic Radiation Damping of Rectangular Composite Plates Subjected to Subsonic Flows," *Journal of Fluids and Structures*, Vol. 8, No. 7, 1994, pp. 737–746.

[16]Wu, S. F., and Maestrello, L., "Responses of Finite Baffled Plate to Turbulent Flow Excitations," *AIAA Journal*, Vol. 33, No. 1, 1995, pp. 13–19.

[17]Smagorinsky, J., "General Circulation Experiments with the Primitive Equations. I. The Basic Experiments," *Monthly Weather Reviews*, Vol. 91, 1963, p. 99.

[18]Moin, P., and Kim, J., "Numerical Investigation of Turbulent Channel Flow," *Journal of Fluid Mechanics*, Vol. 118, May 1982, p. 381.

[19]Germano, M., Piomelli, U., Moin, P., and Cabot, W. H., "A Dynamic Subgrid Scale Eddy Viscosity Model," *Physics of Fluids A*, Vol. 3, No. 7, 1991, p. 1760.

[20]El-hady, N. M., Zang, T. A., and Piomelli, U., "Application of the Dynamic Subgrid-Scale Model to Axisymmetric Transitional Boundary Layer at High Speed," *Physics of Fluids*, Vol. 6, No. 3, 1994, pp. 1299–1309.

[21]Reynolds, O., "An Experimental Investigation of the Circumstances Which Determine Whether the Motion of Water will be Direct or Sinuous and the Law of Resitance in Parallel Channels," *Philosophical Transactions of the Royal Society of London*, Vol. 174, May 1883, p. 935.

[22]Hussain, A. K. M. F., and Reynolds, W. C., "The Mechanics of an Organized Wave in Turbulent Shear Flow," *Journal of Fluid Mechanics*, Vol. 41, Pt. 2, 1970, pp. 241–258.

[23]Hussain, A. K. M. F., and Reynolds, W. C., "The Mechanics of an Organized Wave in Turbulent Shear Flow. Part 2: Experimental Results," *Journal of Fluid Mechanics*, Vol. 54, Pt. 2, 1972, pp. 241–261.

[24]Reynolds, W. C., and Hussain, A. K. M. F., "The Mechanics of an Organized Wave in Turbulent Shear Flow. Part 3: Theoretical Models and Comparisons with Experiments," *Journal of Fluid Mechanics*, Vol. 54, Pt. 2, 1972, pp. 263–288.

[25]Liu, J. T. C., "Developing Large-Scale Wavelike Eddies and the Near Jet Noise Field," *Journal of Fluid Mechanics*, Vol. 62, Pt. 3, 1974, pp. 437–464.

[26]Merkine, L., and Liu, J. T. C., "On the Development of Noise-Producing Large-Scale Wave-Like Eddies in a Plane Turbulent Jet," *Journal of Fluid Mechanics*, Vol. 70, Pt. 2, 1975, pp. 353–368.

[27]Liu, J. T. C., and Merkine, L., "On the Interactions Between Large-Scale Structure and Fine-Grained Turbulence in a Free Shear Flow. I. The Development of Temporal Interactions in the Mean," *Proceedings of the Royal Society of London*, Vol. 352, Jan. 1976, pp. 213–247.

[28]Alper, A., and Liu, J. T. C., "On the Interactions Between Large-Scale Structure and Fine-Grained Turbulence in a Free Shear Flow. II. The Development of Spatial Interactions in the Mean," *Proceedings of the Royal Society of London A*, Vol. 359, Jan. 1978, pp. 497–523.

[29]Gatski, T. B., and Liu, J. T. C., "On the Interactions Between Large-Scale Structure and Fine-Grained Turbulence in a Free Shear Flow. III. A Numerical Solution," *Proceedings of the Royal Society of London A*, Vol. 293, June 1980, p. 473.

[30]Gatski, T. B., "Sound Production due to Large-Scale Coherent Structures," *AIAA Journal*, Vol. 17, No. 6, 1979, pp. 614–621.

[31]Bastin, F., Lafon, P., and Candel, S., "Computation of Jet Mixing Noise from Unsteady Coherent Structures," CEAS/AIAA Paper 95-039, June 1995.

[32]Orzag, S. A., "Turbulent Flow Modeling and Prediction," Inst. for Computer Applications in Sciences and Engineering and Langley Research Center Short Course, March 1994.

[33]Morkovin, M., "Effects of Compressibility on Turbulent Flows," *Mechanique de la Turbulence, Centre National de Recherche Scientifique (CNRS)*, edited by A. Favre, Gordon and Breach, New York, 1962, pp. 367–380.

[34]Sommer, T. P., So, R. M. C., and Gatski, T. B., "Verification of Morkovin's Hypothesis for the Compressible Turbulence Field Using Direct Numerical Simulation Data," AIAA Paper 95-0859, Jan. 1995.

[35]Wilcox, D. C., "Reassessment of the Scale-Determining Equation for Advanced Turbulence Models," *AIAA Journal*, Vol. 26, No. 11, 1988, pp. 1299–1310.

[36]Frendi, A., Maestrello, L., and Ting, L., "An Efficient Model for Coupling Structural Vibrations with Acoustic Radiation," *Journal of Sound and Vibration*, Vol. 182, No. 5, 1995, pp. 741–757.

[37]Rumsey, C., Thomas, J., Warren, G., and Liu, G., "Upwind Navier–Stokes Solutions for Separated Periodic Flows," AIAA Paper 86-0247, Jan. 1986.

[38]Anon., International Mathematical and Statistical Library (IMSL), Version 2.0, Vol. 3, Houston, TX, 1991, p. 1317.

[39]Hoff, C., and Pahl, P. J., "Development of an Implicit Method with Numerical Dissipation from a Generalized Single-Step Algorithm for Structural Dynamics," *Computer Methods in Applied Mechanics and Engineering*, Vol. 67, No. 2, 1988, pp. 367–385.

[40]Maestrello, L., "Radiation from and Panel Response to a Supersonic Turbulent Boundary Layer," *Journal of Sound and Vibration*, Vol. 10, No. 2, 1969, pp. 261–295.

[41]Goodwin, P. W., "An In-Flight Supersonic Turbulent Boundary Layer Surface Pressure Fluctuation Model," High Speed Civil Transport Noise Engineering Group, The Boeing Co., Boeing Document D6-81571, Seattle, WA, March 1994.

[42]Frendi, A., and Maestrello, L., "On the Combined Effect of Mean and Acoustic Excitation on Structural Response and Radiation," *Journal of Vibration and Acoustics*, Vol. 118, Jan. 1997, pp. 1–9.

[43]Lyle, K. H., and Dowell, E. H., "Acoustic Radiation Damping of Flat Rectangular Plates Subjected to Subsonic Flows," *Journal of Fluids and Structures*, Vol. 8, No. 7, 1994, pp. 711–735.